Site-Selective Dissociation upon Sulfur L-edge X-ray Absorption in a Gas-Phase Protonated Peptide

Lucas Schwob,[†[a]] *Simon Dörner,*[†[a]] *Kaan Atak,*[[a]] *Kaja Schubert,*[[a]] *Martin Timm,*[[b]] *Christine Bülow,*[[b]] *Vicente Zamudio-Bayer,*[[b]] *Bernd von Issendorff,*[[c]] *J. Tobias Lau,*[[b][c]] *Simone Techert,*[[a][d]] *and Sadia Bari**[[a]]

[a] Dr. L. Schwob, S. Dörner, Dr. K. Atak, K. Schubert, Prof. Dr. S. Techert, Dr. S. Bari
Deutsches Elektronen-Synchrotron DESY, Notkestrasse 85, 22607 Hamburg (Germany)

[b] M. Timm, Dr. C. Bülow, Dr. V. Zamudio-Bayer, Prof. Dr. J.T. Lau
Abteilung für Hochempfindliche Röntgenspektroskopie, Helmholtz Zentrum Berlin für Materialien und Energie, Albert-Einstein-Strasse.15, 12489 Berlin (Germany)

[c] Prof. Dr. B. von Issendorff, Prof. Dr. J.T.Lau
Physikalisches Institut, Universität Freiburg, Hermann-Herder-Straße 3, 79104 Freiburg (Germany)

[d] Prof. Dr. S. Techert
Institute of X-ray Physics, University of Göttingen, Friedrich-Hund-Platz 1, 37077 Göttingen (Germany)

AUTHOR INFORMATION

† Equal contributors

* Corresponding Authors: lucas.schwob@desy.de sadia.bari@desy

ABSTRACT

Site-selective dissociation induced by core photoexcitation of biomolecules is of key importance for the understanding of radiation damage processes and dynamics, and for its promising use as "chemical scissors" in various applications. However, identifying products of site-selective dissociation in large molecules is challenging at the carbon, nitrogen and oxygen edges because of the high recurrence of these atoms and related chemical groups. In this paper we present the observation of site-selective dissociation at the sulfur L-edge in the gas-phase peptide methionine enkephalin which contains only a single sulfur atom. Near-edge X-ray absorption mass spectrometry has revealed that the resonant S 2p→$\sigma^*_{C\text{-}S}$ excitation of the sulfur contained in the methionine side chain leads to site-selective dissociation, which is not the case after core ionization above the sulfur L-edge. The prospects of such results for the study of charge dynamics in biomolecular systems are discussed.

TOC GRAPHICS

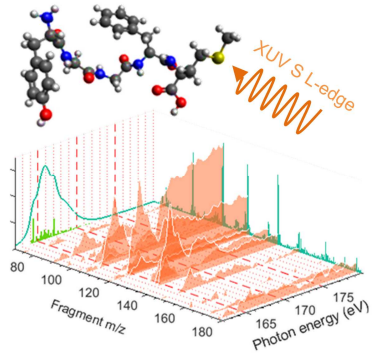

KEYWORDS

Peptide • Electronic structure • Site-selective dissociation • X-ray absorption spectroscopy• Mass spectrometry

The interest in studies on site-selective dissociation (SSD) upon core excitation and ionization of small molecules of increasing complexity has emerged several decades ago[1] with the availability of advanced light sources in the XUV and soft X-ray regime. Core-hole states of molecules composed of atoms with low atomic numbers usually decay via Auger processes, yielding a single or multiple valence hole state. In the case of core excitation, SSD may be expected if the resulting valence hole is localized in the vicinity of the initial core hole and if the fragmentation precedes energy redistribution.[2–8] On the contrary, it has been shown that the character of the dicationic state of a molecule after core ionization prevents SSD.[3] Site-specific absorption as such has brought deep insight into charge dynamics with the help of X-ray free-electron laser (FEL) facilities.[9,10]

Studies on larger, biologically relevant systems like peptides, proteins and oligonucleotides in the frame of radiation damage and the utilization of SSD as "chemical scissors" are of great importance. The former can help understanding the early ultrafast nanoscale physical processes in cancer treatment based on ionizing radiation, while the latter finds application in protein and DNA sequencing allowing for targeted bond cleavage near specific chemical groups or atoms. Earlier experiments by Weinkauf and Schlag,[11–13] followed by Lifshitz *et al.*[14] have been performed using nanosecond UV lasers to resonantly photoionize neutral peptides locally on an absorbing aromatic side chain (Trp, Tyr). On peptides, it has been shown that dissociation on a side opposite to the absorbing chromophore may happen and that two dissociation processes are competing: a fast (fs) hole-driven bond-selective dissociation (although not localized near the absorption site) and a slower statistical fragmentation which follows the intramolecular vibrational redistribution of the energy (IVR, ps timescale) by up to milliseconds.

Gas-phase investigations on photoionization of large mass-selected biomolecules have been carried out only recently by interfacing tandem mass-spectrometers, based on electrospray ionization (ESI) sources and radio-frequency ion traps, with synchrotron and FEL[15] beamlines in both the VUV[16–20] and soft X-ray[21–28] energy range. Near edge X-ray absorption mass spectrometry (NEXAMS)[29], where a mass spectrum of the photofragments is recorded for each photon energy step while scanning across an atomic absorption edge, has proven to be an excellent technique for investigating electronic and geometric structures as well as fragmentation pathways of peptides and proteins. In such systems, carbon, nitrogen and oxygen are the most abundant atoms and are distributed across the whole molecule. Consequently, the bottleneck of investigating SSD upon core excitation or ionization is that the localization of the absorption site cannot be determined. For example, despite the strong resonant excitations to $\pi^*_{C=C}$ in aromatic side chains and to $\pi^*_{C=O}$ in the carbonyl groups of the peptide backbone from C, N and O K-shells observed in peptides,[21,25] the information retrieved is averaged over different absorption sites and the fragmentation pathways are similar.[26] Probing the inner shells of a single sulfur atom included in cysteine or methionine residues as the only excitation site is a promising approach to overcome this obstacle and could pave the way for the study of charge dynamics in large biomolecular systems using soft X-rays in pump-probe experiments.

To test the feasibility of this hypothesis we explored for the first time a singly protonated methionine containing pentapeptide [Met^5]-enkephalin (Tyr-Gly-Gly-Phe-Met, $C_{27}H_{36}N_5O_7S$, m/z = 574, Met-enk in the following) by means of NEXAMS across the sulfur L-edge at the UE52-PGM nanocluster trap beamline[30,31] at the BESSY II synchrotron (HZB Berlin, Germany) (see experimental section). Met-enk is an opioid peptide, only differing from leucine-enkephalin (Tyr-Gly-Gly-Phe-Leu, $C_{28}H_{37}N_5O_7$, Leu-enk) by its C-terminal residue. Leu-enk has been

widely studied as a model peptide in many spectrometric studies.[16,19,29,32–37] The structural similarity of Met-enk to Leu-enk makes it the ideal choice for the investigation of SSD through sulfur core excitation and ionization. However, as the total absorption cross section of a molecule increases with its size, the contrast in cross section for the photon absorption by a single sulfur atom is drastically decreased. The contrast in absorption strength at the S 2p orbital against another site in the peptide can be estimated considering the sum of the tabulated atomic cross sections[38] for C, N, O and H, $\sigma(C_{27}H_{36}N_5O_7)$, and the reported absolute absorption cross section for H_2S at the S 2p inner-shell region, σ(S). One can expect $\sigma(S):\sigma(C_{27}H_{36}N_5O_7)$ ratios of 9:91 for the absorption strength for the S 2p resonant excitation at 166.7 eV and of 11:89 for the S 2p ionization at 180 eV. In the following, we will first discuss the features observed in the NEXAMS spectrum of Met-enk across the sulfur L-edge and then detail the mass spectra where evidence for SSD has been found. The trapping parameters of the nanocluster trap were optimized to a m/z of 60 to 200, where most of the fragments for this peptide are expected.[16,19,29,39] As all fragments cannot be detected at once, we discuss the absorption spectra in the following in terms of ion yield rather than total ion yield.

Figure 1 shows the ion yield spectra for both enkephalins at the sulfur L-edge, between photon energies of 155 and 180 eV. The spectra were obtained by summing up the yields of the observed fragments in the mass spectra and were normalized by the photon flux (see **Figure 4**). For Leu-enk, which contains no sulfur atom, the ion yield shows no resonance and declines due to the decrease in photoabsorption cross section by a factor 2 over the studied photon energy range. Met-enk though, shows resonant excitation peaks centered at 166 eV. These features are superimposed on a baseline caused by the fragmentation of the peptide following non-resonant photoabsorption by the valence orbitals. At 166 eV, the contribution to the fragmentation yield

resulting from the absorption at the sulfur atom is ~13 % which is in agreement with the anticipated ratios calculated from the absorption cross sections.

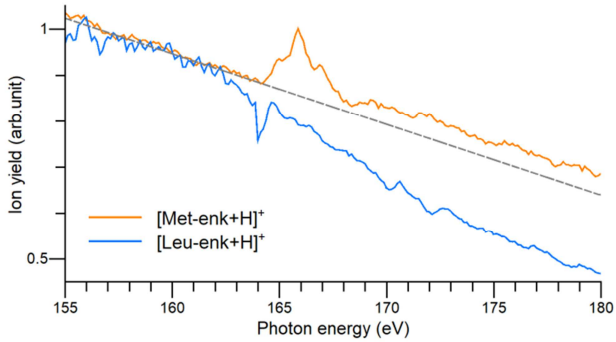

Figure 1. Ion yield spectra for protonated $[Met\text{-}enk+H]^+$ and $[Leu\text{-}enk+H]^+$ around the sulfur L-edge, adjusted at 160 eV. The ion yield is obtained by integrating all fragment peaks in the mass spectra for each photon energy. The dip observed at 164 eV for $[Leu\text{-}enk+H]^+$ is due to precursor ion intensity fluctuations. The dashed line is a linear extrapolation of the pre-edge trend of $[Met\text{-}enk+H]^+$ as used for baseline correction.

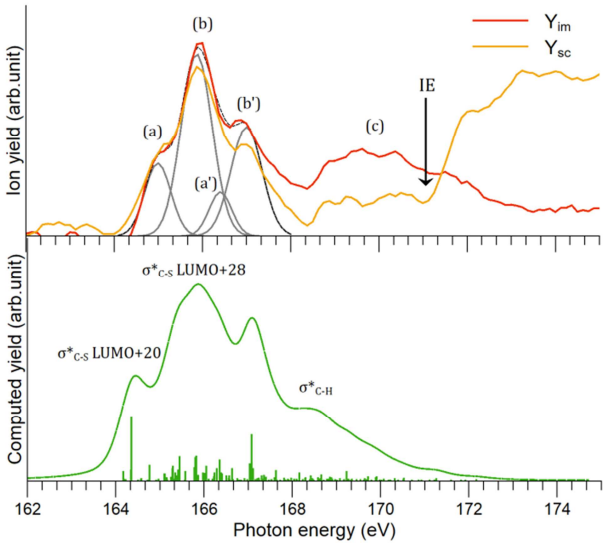

Figure 2. Top: baseline-corrected ion yield spectrum for the tyrosine immonium (Y_{im}) and side chain (Y_{sc}) fragments. Gaussian fitting leads to four main transitions of width 0.8 eV (FWHM)

centered at the energies (a) 164.9 eV ($2p_{3/2}$→LUMO+20), (a') 166.4 eV ($2p_{1/2}$→LUMO+20), (b) 165.9 eV ($2p_{3/2}$→LUMO+28) and (b') 167.0 eV ($2p_{1/2}$→LUMO+28). Bottom: DFT/ROCIS calculation of the transitions from sulfur 2p to unoccupied molecular orbitals. The green curve is obtained by a 0.68 eV (FWHM) pseudo-Voigt function (0.3 eV FWHM Lorentzian with 0.5 eV Gaussian functions) broadening of the transition lines. The computed spectrum is shifted by 6.7 eV to fit the experimental data.

Examining the ion yields of individual fragments allows for extracting more detailed information. The top panel of **Figure 2** shows the baseline-corrected ion yield spectra for the tyrosine immonium (Y_{im}) and side chain (Y_{sc}) fragments (see **Figure 4** and discussion). For each fragment ion yield, the baseline subtraction is made using a linear extrapolation of the pre-edge trend of the individual spectrum, as shown in example in the **Figure 1**. Here, data from [Leu-enk+H]$^+$ cannot be used as baseline because the nature of the fragments and their yield may differ from [Met-enk+H]$^+$ due to electronic and geometric structural differences. While only resonant excitations (peaks (a), (b) and (c)) contribute to the ion yield of Y_{im}, the yield of Y_{sc} shows a strong increase upon core ionization. An ionization energy of ~170.9 eV is extracted from these data, consistent with measurements on small sulfur-containing molecules.[40] In order to assess the probed molecular orbitals of the resonant excitations, density functional theory / restricted open-shell single excitation configuration interaction (DFT/ROCIS) calculations, including spin-orbit coupling (see computational section), were conducted for protonated Met-enk. In these calculations, the additional proton was positioned at the N-terminus, as was determined for protonated Leu-enk[35]. Gaussian fitting of the experimental data gives rise to four transitions of full width at half maximum (FWHM) 0.8 eV and centered at 164.9, 165.9, 166.4 and 167 eV. As the lifetime broadening is expected to be 0.3 eV[41] and the photon energy

bandwidth is of 0.077 eV, the ~0.4 eV remaining broadening of the transitions mainly originates from additional vibrational excitations. Therefore the broadening of the transition lines of the calculated absorption spectrum have been made with pseudo-Voigt functions from the linear combination of 0.3 eV width Lorentzian with 0.5 eV width Gaussian functions. **Figure 2** shows a good agreement between the ion yield spectrum (top panel) and the convoluted absorption spectrum (bottom panel). By comparison with the calculations four main resonances have been assigned to transitions from the two spin orbit split of the S 2p levels $2p_{3/2}$ and $2p_{1/2}$ to two unoccupied molecular orbitals mainly involving antibonding $\sigma^*_{C\text{-}S}$ states: $2p_{3/2}$→LUMO+20 (a), $2p_{1/2}$ →LUMO+20 (a'), $2p_{3/2}$→LUMO+28 (b) and $2p_{1/2}$→ LUMO+28 (b') where the LUMO is the Lowest Unoccupied Molecular Orbital and the +20 or +28 relate to the molecular orbital number relative to the LUMO. The average energy separation between the two $2p_{3/2}$ and $2p_{1/2}$ states is ~1.3 eV, close to the expected value of 1.16 eV for the spin-orbit splitting of the S 2p orbital.[42] At higher energies, the broader feature centered at 168-170 eV cannot be assigned to a specific antibonding orbital but mainly contains molecular orbitals of $\sigma^*_{C\text{-}H}$ character in the proximity of the methionine side chain. The LUMO+20 and LUMO+28, depicted in **Figure 3**, are the least energetic unoccupied molecular orbitals involving the sulfur atom. Contributions of $\sigma^*_{O\text{-}H}$ located in the COOH group of the LUMO+20 and $\sigma^*_{C\text{-}H}$ in the phenyl ring of the phenylalanine of the LUMO+28 are weaker than the $\sigma^*_{C\text{-}S}$ contribution by a tenth and a half respectively. Contrary to the observations at the C, N and O K-edges for peptides[24], here no strong transitions to $\pi^*_{C=O}$ or $\pi^*_{C=C}$ states of neighboring chemical groups have been identified in our calculations. It is worth noting that in the case of gas-phase[43] and condensed-phase[44] methionine upon sulfur K-edge excitation, two molecular orbitals of similar character are probed, corresponding in these cases to the LUMO and LUMO+1. Additionally, our ion yield spectrum

for $[Met\text{-}enk+H]^+$ is in very good agreement with the X-ray absorption spectrum of methionine powder[45] and the photo-electron yield spectrum of isolated H_2S molecule[46] measured at the sulfur L-edge. This suggests that the proximity of other residues has only little effect on the transitions probed at the sulfur L-edge.

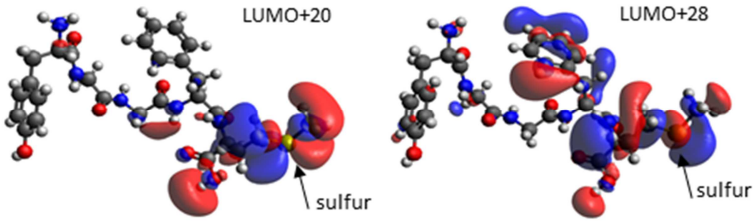

Figure 3. Calculated electronic densities of the two main molecular orbitals probed at the sulfur L-edge. The LUMO+20 and LUMO+28 correspond to the first two unoccupied molecular orbitals involving the sulfur atom of the methionine side chain. Details of the atomic orbital contributions can be found in the supporting information.

Despite the small contrast in absorption cross section, evidence for the photoabsorption at a sulfur atom in a large peptide has been observed and the different transitions accessible upon sulfur L-edge photoabsorption in $[Met\text{-}enk+H]^+$ have been identified. Still, evidence for site-selective dissociation can only be found in the photodissociation mass spectra. The top panel of **Figure 4** shows the mass spectrum obtained at 166 eV photon energy *i.e.* on the ($2p_{3/2}$→LUMO+28) (b) resonance. Fragments are labelled according to the peptide fragment nomenclature established by Roepstorff and Fohlman[47] and Biemann[48] (see **Figure 5**). Briefly, the most intense peaks correspond to the immonium ions (*im*) and side chain fragments (*sc*) of the aromatic residues phenylalanine (F_{im}, m/z = 120 and F_{sc}, m/z = 91 and 77) and tyrosine (Y_{im}, m/z = 136 and Y_{sc}, m/z = 107, 91 and 77). The immonium ion and protonated side chain

fragments of the methionine (M_{im}, m/z = 104 and M_{sc}, m/z = 75) are also produced, as well as several internal fragments. This spectrum resembles the spectra of protonated $[Leu\text{-}enk+H]^+$ obtained upon carbon K-edge photoabsorption[29] and keV ion-induced dissociation.[39] Indeed, as the relative increase in fragmentation following the photon absorption at the sulfur is only ~13 % most of the fragmentation is the result of non-resonant absorption.

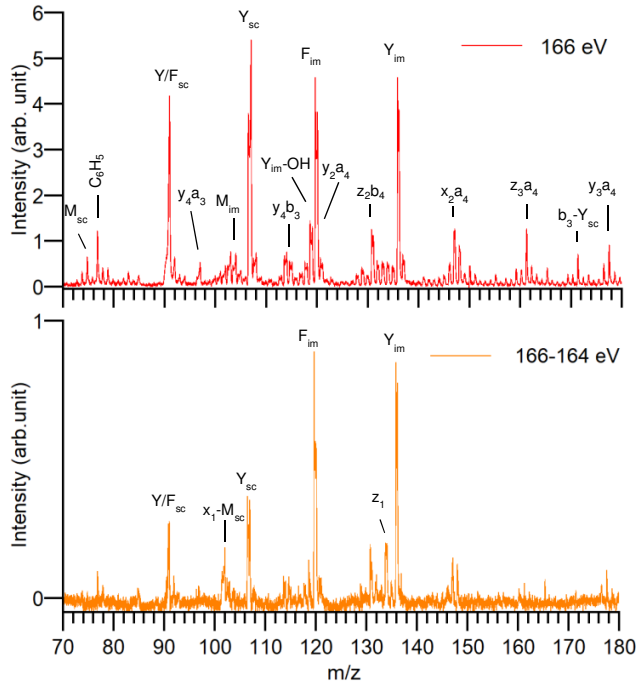

Figure 4. Top: photodissociation mass spectrum of $[Met\text{-}enk+H]^+$ at a photon energy of 166 eV. Bottom: difference spectrum after subtraction of the mass spectra at 166 eV (on resonance) – 164 eV (below resonance). For intensity comparison, the same scale is used in both spectra. Letters M, Y and F stand for methionine, tyrosine and phenylalanine respectively. "sc" is for side chain fragment and "im" is for immonium ion.

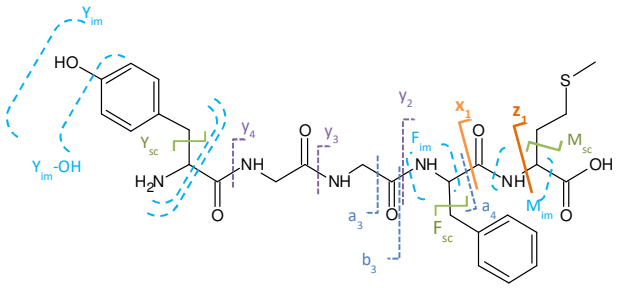

Figure 5. Met-enk chemical structure and cleavage sites.

Without coincidence measurements with the Auger electron emitted after S 2p electron excitation, one way to differentiate the result of the sulfur absorption from non-resonant absorption is to rule out the contribution of the non-resonant absorption. For this purpose **Figure 4**-bottom shows the difference spectrum calculated by subtracting the below-resonance (164 eV) spectrum from the on-resonance (166 eV) spectrum. The obtained mass spectrum includes only dissociation resulting from resonant absorption at the sulfur L-edge. Interestingly, the fragmentation pattern appears similar to the one at 166 eV, the main fragments still being the tyrosine and phenylalanine immonium ions. To evaluate how the absorption at the sulfur specifically contributes to the production of each fragment, in **Figure 6** is plotted the increase of the fragmentation yield induced by the resonant photon absorption at the sulfur L-edge (the difference spectrum) relatively to the yield of the non-resonant absorption (164 eV spectrum) for each fragment. The same operation has been made for the spectrum obtained after core ionization (CI), at 172 eV. At the resonance, the first striking result is the ~65 % increase in yield for the two fragments z_1 and x_1-M_{sc} (loss of 74 Da, C_3H_6S), both situated at the C-terminal side of the peptide, where the methionine residue, and thus the sulfur atom, is located. In contrast, all the other fragment yields exhibit an averaged relative increase of (13 ± 6) %. Moreover, despite the absorption at the sulfur atom, the methionine immonium ion M_{im} and side chain fragment M_{sc}

show a particularly weak yield increase of 8 % and 2 %, respectively. Whereas the LUMO+28 has some $\sigma^*_{C\text{-}H}$ character on the phenyl ring of the phenylalanine residue, the yields of phenylalanine-related fragments do not show any significant increase in comparison to other fragments. Similarly, we do not observe fragments related to the cleavage of the CH_2-S nor S-CH_3 bonds although we are probing the C-S anti-bounding orbitals which would weaken these bounds in the methionine side chain. Interestingly, upon core ionization, the z_1 fragment is absent and the yield of the x_1-M_{sc} fragment decreases by a factor of ten. These two fragments seem to be exclusive to the resonant S 2p excitation followed by Auger decay and the processes by which they are produced are hindered in the double-hole state after core ionization and Auger decay. At 172 eV, the relative yield increase drops to (6 ± 5) % in average.

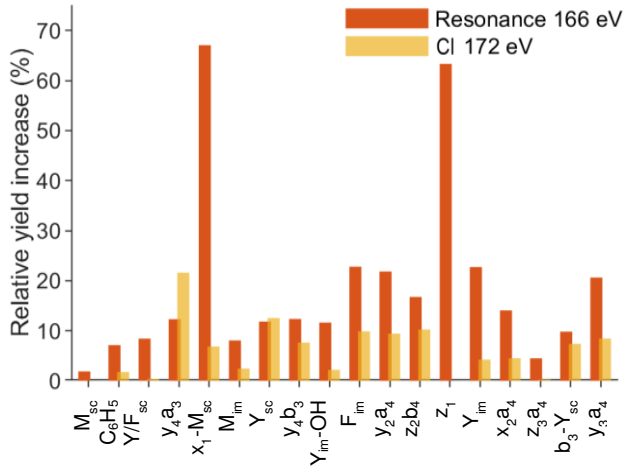

Figure 6. Increase of the fragmentation yield for each fragment due to absorption at the sulfur at the resonance (166 eV, orange bars) and above the sulfur L-edge¸ *i.e.* after core ionization (CI) (172 eV, yellows bars) relative to the fragmentation yield of the pre-edge non-resonant absorption.

The high yield increase for the z_1 and x_1-M_{sc} fragments in comparison to all other fragments proves local site-selective dissociations. Peptide fragments of z- and x-type are known to be

formed *via* radical (valence hole)-induced processes in radical cations,[49–51] in contrast to the regular b/y-type fragments observed in collision-induced dissociation (CID).[52] Similarly, side chain losses following photo ionization have been identified recently as being caused by the valence hole remaining on the peptide after ionization.[26] In particular the neutral loss of C_3H_6S from the methionine side chain has already been observed for methionine-containing peptides upon VUV photoionization[53] and radical-induced dissociation.[54–56] This side chain loss involves the cleavage of the C_α-C_β bond and leaves the radical on the backbone of the peptide which can thus undergo further radical-induced dissociations in a cascade fashion. In the present case, this would suggest that the valence hole resulting from the Auger decay initially remains in the vicinity of the sulfur atom and then migrates from the side chain towards the peptide backbone, consequently producing the z_1 and x_1-M_{sc} fragments, the latter involving cascade dissociations. The other fragments show, however, a different behavior. Their similar relative yield increase and the fact that fragments remote from the sulfur, such as Y_{im} on the opposite side of the peptide, are equally produced, indicate that the peptide may also undergo a statistical fragmentation following a fast IVR.

In conclusion, we have shown that resonant sulfur 2p photon absorption on a pentapeptide in the gas phase can be observed with a contrast of about ten percent to non-resonant absorption and also leads to site-selective dissociation pathways. Near edge X-ray absorption mass spectrometry proved to be a suited method for suchlike investigations by providing information about both the electronic structure in the proximity of the probed sulfur atom and the subsequent dissociation pathways. We have evidenced that two processes are competing following the excitation of a sulfur 2p electron: SSD induced by the valence hole in the vicinity of the sulfur atom and statistical fragmentation following IVR. However, SSD is not observed upon core

ionization. In this case, the presence of multiple positive charges might induce a strong coulombic repulsion leading to different fragmentation pathways. The following open questions have now to be addressed: To which extent in terms of peptide size can site-specific dissociation still be observed? How do neighboring residues affect the local radical migration and does the radical preferentially migrate towards the N- or C- terminus or another specific chemical group? Which processes govern the fragmentation of such systems after core ionization? Are different timescales involved for SSD and IVR? Testing the region-specificity of these processes in custom-made peptides with the methionine residue placed at different positions will be addressed in future experiments. It is worth noting here that a similar approach could also be envisioned for the study of oligonucleotides by probing the phosphorus atom of the backbone. This topic is now opened to more systematic studies to shed light on these processes. Eventually, this should pave the way for pump-probe studies on large biomolecules in the gas phase at XUV and soft X-ray FEL facilities. Valuable information on the dynamics of charge migration (proton or radical) could thus be obtained, yielding a considerable step forward in the understanding of the physical processes occurring in biomolecules.

EXPERIMENTAL SECTION

The experiments have been carried out at the Nanocluster trap endstation at the UE52_PGM beamline[30,31] at the BESSY II synchrotron (HZB Berlin, Germany). The sample ions were produced by electrospray ionization and guided through a radio-frequency hexapole ion guide to a quadrupole mass filter where the precursor ions were mass-to-charge selected. After passing a 90° bender, the ions were buffer-gas cooled, accumulated and stored in a cryogenic linear ion trap at 18 K. The ions were exposed to soft X-ray radiation for 100 ms in the trap and the cation products were mass analyzed in a reflectron time-of-flight mass spectrometer. Due to the

specificity of the setup, the mass resolution is not constant over the whole mass range. The mass resolution m/Δm is of 350 at m/z = 77, 207 at m/z = 120 and 700 at m/z = 177. The exit slit of the monochromator was set to an energy bandwidth of 77 meV. Energy scans were performed by steps of 125 meV. Leucine-enkephalin and [Met^5]-enkephalin acetate salt hydrate (purity ≥ 95 %), purchased from Sigma-Aldrich, were used without further purification. The peptides were prepared at 30 μM in 1:1 water/methanol solutions with 1% volume formic acid.

COMPUTATIONAL METHOD

The calculations were carried out with the ORCA program package.[57] Molecular geometry optimizations were performed using the B3LYP[58,59] density functional method with the Ahlrichs TZVP[60] basis set. Transition energies and moments for sulfur L-edge were calculated with DFT/ROCIS using the same basis set. For DFT/ROCIS calculations, the B3LYP functional together with the parameters c1 = 0.18, c2 = 0.20, and c3 = 0.40 was applied.[61] During the calculations, the resolution of identity[62–66] approximation was used employing the Autoaux generation procedure.[67] Numerical integrations during the DFT calculations were performed on a dense grid (ORCA grid4). In all calculations, relativistic effects were taken into account using zeroth-order regular approximation (ZORA).[68] The geometry calculations had no symmetry constraint. Vibronic effects were not taken into account in the calculations.

ASSOCIATED CONTENT

Calculated molecular orbitals LUMO+20 and LUMO+28 with corresponding atomic contribution, as well as fragment masses and attributions can be found in the **Supporting Information.**

AUTHOR INFORMATION

The authors declare no competing financial interests.

ACKNOWLEDGMENT

We thank HZB for the allocation of synchrotron radiation beamtime at beamline UE52-PGM. L.S., S.D., K.S. and S.B. were supported by the Helmholtz Initiative and Networking Fund through the Young Investigators Group Program. K.S., S.T. and S.B. acknowledge support from the Deutsche Forschungsgemeinschaft, project B03/SFB755. The endstation at UE52-PGM is partially supported by BMBF grant 05K16VF1.

REFERENCES

(1) Eberhardt, W.; Sham, T. K.; Carr, R.; Krummacher, S.; Strongin, M.; Weng, S. L.; Wesner, D. Site-Specific Fragmentation of Small Molecules Following Soft x-Ray Excitation. *Phys. Rev. Lett.* **1983**, *50* (14), 1038–1041. https://doi.org/10.1103/PhysRevLett.50.1038.

(2) Miron, C.; Simon, M.; Leclercq, N.; Hansen, D. L.; Morin, P. Site-Selective Photochemistry of Core Excited Molecules: Role of the Internal Energy. *Phys. Rev. Lett.* **1998**, *81* (19), 4104–4107. https://doi.org/10.1103/PhysRevLett.81.4104.

(3) Inhester, L.; Oostenrijk, B.; Patanen, M.; Kokkonen, E.; Southworth, S. H.; Bostedt, C.; Travnikova, O.; Marchenko, T.; Son, S. K.; Santra, R.; et al. Chemical Understanding of the Limited Site-Specificity in Molecular Inner-Shell Photofragmentation. *J. Phys. Chem. Lett.* **2018**, *9* (5), 1156–1163. https://doi.org/10.1021/acs.jpclett.7b03235.

(4) Bolognesi, P.; Kettunen, J. A.; Cartoni, A.; Richter, R.; Tosic, S.; Maclot, S.; Rousseau, P.; Delaunay, R.; Avaldi, L. Site- and State-Selected Photofragmentation of 2Br-Pyrimidine. *Phys. Chem. Chem. Phys.* **2015**, *17* (37), 24063–24069. https://doi.org/10.1039/c5cp02601f.

(5) Takahashi, O.; Kooser, K.; Ha, D. T.; Myllynen, H.; Laksman, J.; Rachlew, E.; Kukk, E. Site-Selective Bond Scission of Methylbenzoate Following Core Excitation. *Phys. Chem.*

Chem. Phys. **2018**, *20* (14), 9591–9599. https://doi.org/10.1039/C7CP08428E.

(6) Nagaoka, S. I.; Fukuzawa, H.; Prümper, G.; Takemoto, M.; Takahashi, O.; Yamaguchi, K.; Kakiuchi, T.; Tabayashi, K.; Suzuki, I. H.; Harries, J. R.; et al. A Study to Control Chemical Reactions Using Si:2p Core Ionization: Site-Specific Fragmentation. *J. Phys. Chem. A* **2011**, *115* (32), 8822–8831. https://doi.org/10.1021/jp203664r.

(7) Chiang, Y. J.; Huang, W. C.; Ni, C. K.; Liu, C. L.; Tsai, C. C.; Hu, W. P. NEXAFS Spectra and Specific Dissociation of Oligo-Peptide Model Molecules. *AIP Adv.* **2019**, *9* (8), 085023. https://doi.org/10.1063/1.5112151.

(8) Schmelz, H. C.; Reynaud, C.; Simon, M.; Nenner, I. Site-Selective Fragmentation in Core-Excited Bromo-Chloro-Alkanes [$Br(CH_2)_nCl$]. *J. Chem. Phys.* **1994**, *101* (5), 3742–3749. https://doi.org/10.1063/1.467558.

(9) Erk, B.; Boll, R.; Trippel, S.; Anielski, D.; Foucar, L.; Rudek, B.; Epp, S. W.; Coffee, R.; Carron, S.; Schorb, S.; et al. Imaging Charge Transfer in Iodomethane upon X-Ray Photoabsorption. *Science.* **2014**, *345* (6194), 288–291. https://doi.org/10.1126/science.1253607.

(10) Boll, R.; Erk, B.; Coffee, R.; Trippel, S.; Kierspel, T.; Bomme, C.; Bozek, J. D.; Burkett, M.; Carron, S.; Ferguson, K. R.; et al. Charge Transfer in Dissociating Iodomethane and Fluoromethane Molecules Ionized by Intense Femtosecond X-Ray Pulses. *Struct. Dyn.* **2016**, *3* (4). https://doi.org/10.1063/1.4944344.

(11) Weinkauf, R.; Schanen, P.; Yang, D.; Soukara, S.; Schlag, E. W. Elementary Processes in Peptides: Electron Mobility and Dissociation in Peptide Cations in the Gas Phase. *J. Phys. Chem.* **1995**, *99* (28), 11255–11265. https://doi.org/10.1021/j100028a029.

(12) Weinkauf, R.; Schanen, P.; Metsala, A.; Schlag, E. W.; Bürgle, M.; Kessler, H. Highly Efficient Charge Transfer in Peptide Cations in the Gas Phase: Threshold Effects and Mechanism. *J. Phys. Chem.* **1996**, *100* (47), 18567–18585. https://doi.org/10.1021/jp960926m.

(13) Schlag, E. W.; Selzle, H. L.; Schanen, P.; Weinkauf, R.; Levine, R. D. Dissociation

Kinetics of Peptide Ions. *J. Phys. Chem. A* **2006**, *110* (27), 8497–8500. https://doi.org/10.1021/jp0557641.

(14) Hu, Y.; Hadas, B.; Davidovitz, M.; Balta, B.; Lifshitz, C. Does IVR Take Place Prior to Peptide Ion Dissociation? *J. Phys. Chem. A* **2003**, *107* (34), 6507–6514. https://doi.org/10.1021/jp030275b.

(15) Schlathölter, T.; Reitsma, G.; Egorov, D.; Gonzalez-Magaña, O.; Bari, S.; Boschman, L.; Bodewits, E.; Schnorr, K.; Schmid, G.; Schröter, C. D.; et al. Multiple Ionization of Free Ubiquitin Molecular Ions in Extreme Ultraviolet Free-Electron Laser Pulses. *Angew. Chemie - Int. Ed.* **2016**, *55* (36), 10741–10745. https://doi.org/10.1002/anie.201605335.

(16) Bari, S.; Gonzalez-Magaña, O.; Reitsma, G.; Werner, J.; Schippers, S.; Hoekstra, R.; Schlathölter, T. Photodissociation of Protonated Leucine-Enkephalin in the VUV Range of 8-40 eV. *J. Chem. Phys.* **2011**, *134* (024314). https://doi.org/10.1063/1.3515301.

(17) Gonzalez-Magaña, O.; Reitsma, G.; Bari, S.; Hoekstra, R.; Schlathölter, T. Length Effects in VUV Photofragmentation of Protonated Peptides. *Phys. Chem. Chem. Phys.* **2012**, *14* (13), 4351–4354. https://doi.org/10.1039/c2cp23470j.

(18) Egorov, D.; Hoekstra, R.; Schlathölter, T. A Comparative VUV Absorption Mass-Spectroscopy Study on Protonated Peptides of Different Size. *Phys. Chem. Chem. Phys.* **2017**, *19* (31), 20608–20618. https://doi.org/10.1039/C7CP03203J.

(19) Ranković, M. L.; Canon, F.; Nahon, L.; Giuliani, A.; Milosavljević, A. R. VUV Action Spectroscopy of Protonated Leucine-Enkephalin Peptide in the 6-14 eV Range. *J. Chem. Phys.* **2015**, *143* (244311). https://doi.org/10.1063/1.4939080.

(20) Canon, F.; Milosavljević, A. R.; van der Rest, G.; Réfrégiers, M.; Nahon, L.; Sarni-Manchado, P.; Cheynier, V.; Giuliani, A. Photodissociation and Dissociative Photoionization Mass Spectrometry of Proteins and Noncovalent Protein-Ligand Complexes. *Angew. Chemie - Int. Ed.* **2013**, *52* (32), 8377–8381. https://doi.org/10.1002/anie.201304046.

(21) Milosavljević, A. R.; Canon, F.; Nicolas, C.; Miron, C.; Nahon, L.; Giuliani, A. Gas-Phase

Protein Inner-Shell Spectroscopy by Coupling an Ion Trap with a Soft X-Ray Beamline. *J. Phys. Chem. Lett.* **2012**, *3* (9), 1191–1196. https://doi.org/10.1021/jz300324z.

(22) Giuliani, A.; Milosavljević, A. R.; Hinsen, K.; Canon, F.; Nicolas, C.; Réfrégiers, M.; Nahon, L. Structure and Charge-State Dependence of the Gas-Phase Ionization Energy of Proteins. *Angew. Chemie - Int. Ed.* **2012**, *51* (38), 9552–9556. https://doi.org/10.1002/anie.201204435.

(23) Milosavljević, A. R.; Nicolas, C.; Ranković, M. L.; Canon, F.; Miron, C.; Giuliani, A. K-Shell Excitation and Ionization of a Gas-Phase Protein: Interplay between Electronic Structure and Protein Folding. *J. Phys. Chem. Lett.* **2015**, *6* (16), 3132–3138. https://doi.org/10.1021/acs.jpclett.5b01288.

(24) Egorov, D.; Schwob, L.; Lalande, M.; Hoekstra, R.; Schlathölter, T. Near Edge X-Ray Absorption Mass Spectrometry of Gas Phase Proteins: The Influence of Protein Size. *Phys. Chem. Chem. Phys.* **2016**, *18* (37), 26213–26223. https://doi.org/10.1039/C6CP05254A.

(25) Egorov, D.; Bari, S.; Boll, R.; Dörner, S.; Deinert, S.; Techert, S.; Hoekstra, R.; Zamudio-Bayer, V.; Lindblad, R.; Bülow, C.; et al. Near-Edge Soft X-Ray Absorption Mass Spectrometry of Protonated Melittin. *J. Am. Soc. Mass Spectrom.* **2018**, *29* (11), 2138–2151. https://doi.org/10.1007/s13361-018-2035-6.

(26) Schwob, L.; Lalande, M.; Egorov, D.; Rangama, J.; Hoekstra, R.; Vizcaino, V.; Schlathölter, T.; Poully, J.-C. Radical-Driven Processes within a Peptidic Sequence of Type I Collagen upon Single-Photon Ionisation in the Gas Phase. *Phys. Chem. Chem. Phys.* **2017**, *19* (34), 22895–22904. https://doi.org/10.1039/C7CP03376A.

(27) Schwob, L.; Lalande, M.; Rangama, J.; Egorov, D.; Hoekstra, R.; Pandey, R.; Eden, S.; Schlathölter, T.; Vizcaino, V.; Poully, J.-C. Single-Photon Absorption of Isolated Collagen Mimetic Peptides and Triple-Helix Models in the VUV-X Energy Range. *Phys. Chem. Chem. Phys.* **2017**, *19* (28), 18321–18329. https://doi.org/10.1039/C7CP02527K.

(28) Bari, S.; Egorov, D.; Jansen, T. L. C.; Boll, R.; Hoekstra, R.; Techert, S.; Zamudio-Bayer,

V.; Bülow, C.; Lindblad, R.; Leistner, G.; et al. Soft X-Ray Spectroscopy as a Probe for Gas-Phase Protein Structure: Electron Impact Ionization from Within. *Chem. - A Eur. J.* **2018**, *24* (30), 7631–7636. https://doi.org/10.1002/chem.201801440.

(29) Gonzalez-Magaña, O.; Reitsma, G.; Tiemens, M.; Boschman, L.; Hoekstra, R.; Schlathölter, T. Near-Edge X-Ray Absorption Mass Spectrometry of a Gas-Phase Peptide. *J. Phys. Chem. A* **2012**, *116* (44), 10745–10751. https://doi.org/10.1021/jp307527b.

(30) Hirsch, K.; Lau, J. T.; Klar, P.; Langenberg, A.; Probst, J.; Rittmann, J.; Vogel, M.; Zamudio-Bayer, V.; Möller, T.; von Issendorff, B. X-Ray Spectroscopy on Size-Selected Clusters in an Ion Trap: From the Molecular Limit to Bulk Properties. *J. Phys. B At. Mol. Opt. Phys.* **2009**, *42* (154029). https://doi.org/10.1088/0953-4075/42/15/154029.

(31) Niemeyer, M.; Hirsch, K.; Zamudio-Bayer, V.; Langenberg, A.; Vogel, M.; Kossick, M.; Ebrecht, C.; Egashira, K.; Terasaki, A.; Möller, T.; et al. Spin Coupling and Orbital Angular Momentum Quenching in Free Iron Clusters. *Phys. Rev. Lett.* **2012**, *108* (057201). https://doi.org/10.1103/PhysRevLett.108.057201.

(32) Herburger, A.; van der Linde, C.; Beyer, M. K. Photodissociation Spectroscopy of Protonated Leucine Enkephalin. *Phys. Chem. Chem. Phys.* **2017**, *19* (17), 10786–10795. https://doi.org/10.1039/c6cp08436b.

(33) Reitsma, G.; Gonzalez-Magaña, O.; Versolato, O.; Door, M.; Hoekstra, R.; Suraud, E.; Fischer, B.; Camus, N.; Kremer, M.; Moshammer, R.; et al. Femtosecond Laser Induced Ionization and Dissociation of Gas-Phase Protonated Leucine Enkephalin. *Int. J. Mass Spectrom.* **2014**, *365–366*, 365–371. https://doi.org/10.1016/j.ijms.2014.01.004.

(34) Moon, J. H.; Yoon, S. H.; Bae, Y. J.; Kim, M. S. Dissociation Kinetics of Singly Protonated Leucine Enkephalin Investigated by Time-Resolved Photodissociation Tandem Mass Spectrometry. *J. Am. Soc. Mass Spectrom.* **2010**, *21* (7), 1151–1158. https://doi.org/10.1016/j.jasms.2010.03.025.

(35) Polfer, N. C.; Oomens, J.; Suhai, S.; Paizs, B. Infrared Spectroscopy and Theoretical Studies on Gas-Phase Protonated Leu-Enkephalin and Its Fragments: Direct Experimental

Evidence for the Mobile Proton. *J. Am. Chem. Soc.* **2007**, *129* (18), 5887–5897. https://doi.org/10.1021/ja068014d.

(36) Cai, X.; Dass, C. Structural Characterization of Methionine and Leucine Enkephalins by Hydrogen/Deuterium Exchange and Electrospray Ionization Tandem Mass Spectrometry. *Rapid Commun. Mass Spectrom.* **2005**, *19* (1), 1–8. https://doi.org/10.1002/rcm.1739.

(37) Tabarin, T.; Antoine, R.; Broyer, M.; Dugourd, P. Specific Photodissociation of Peptides with Multi-Stage Mass Spectrometry. *Rapid Commun. Mass Spectrom.* **2005**, *19* (20), 2883–2892. https://doi.org/10.1002/rcm.2124.

(38) Yeh, J. J.; Lindau, I. Atomic Subshell Photoionization Cross Sections and Asymmetry Parameters: $1 \leqslant Z \leqslant 103$. *At. Data Nucl. Data Tables* **1985**, *32* (1), 1–155. https://doi.org/10.1016/0092-640X(85)90016-6.

(39) Bari, S.; Hoekstra, R.; Schlathölter, T. Peptide Fragmentation by keV Ion-Induced Dissociation. *Phys. Chem. Chem. Phys.* **2010**, *12*, 3376–3383. https://doi.org/10.1039/b924145k.

(40) Coville, M.; Thomas, T. D. Sulfur 2p Ionization Energies of H_2S, OCS, SO_2, and CS_2. *J. Electron Spectros. Relat. Phenomena* **1995**, *71* (1), 21–23. https://doi.org/10.1016/0368-2048(94)02257-7.

(41) Hudson, E.; Shirley, D. A.; Domke, M.; Remmers, G.; Puschmann, A.; Mandel, T.; Xue, C.; Kaindl, G. High-Resolution Measurements of Nearedge Resonances in the Core-Level Photoionization Spectra of SF_6. *Phys. Rev. A* **1993**, *47* (1), 361–373. https://doi.org/https://doi.org/10.1103/PhysRevA.47.361.

(42) Svensson, S.; Naves De Brito, A.; Keane, M. P.; Correia, N.; Karlsson, L. Observation of an Energy Shift in the S $2p_{3/2}$ - S $2p_{1/2}$ Spin-Orbit Splitting between X-Ray Photoelectron and Auger-Electron Spectra for the H_2S Molecule. *Phys. Rev. A* **1991**, *43* (11), 6441–6443. https://doi.org/10.1103/PhysRevA.43.6441.

(43) Behyan, S.; Hu, Y.; Urquhart, S. G. Sulfur 1s Near-Edge X-Ray Absorption Fine Structure

(NEXAFS) of Thiol and Thioether Compounds. *J. Chem. Phys.* **2011**, *134* (244304). https://doi.org/10.1063/1.3602218.

(44) Mijovilovich, A.; Pettersson, L. G. M.; Mangold, S.; Janousch, M.; Susini, J.; Salome, M.; De Groot, F. M. F.; Weckhuysen, B. M. The Interpretation of Sulfur K-Edge XANES Spectra: A Case Study on Thiophenic and Aliphatic Sulfur Compounds. *J. Phys. Chem. A* **2009**, *113* (12), 2750–2756. https://doi.org/10.1021/jp806823c.

(45) Kasrai, M.; Brown, J. R.; Bancroft, G. M.; Yin, Z.; Tan, K. H. Sulphur Characterization in Coal from X-Ray Absorption Near Edge Spectroscopy. *Int. J. Coal Geol.* **1996**, *32* (1–4), 107–135. https://doi.org/10.1016/S0166-5162(96)00033-X.

(46) Le Guen, K.; Miron, C.; Ćolin, D.; Guillemin, R.; Leclercq, N.; Simon, M.; Morin, P.; Mocellin, A.; Björneholm, O.; Naves De Brito, A.; et al. H_2S Ultrafast Dissociation Probed by Energy-Selected Resonant Auger Electron-Ion Coincidence Measurements. *J. Chem. Phys.* **2007**, *127* (11). https://doi.org/10.1063/1.2776265.

(47) Roepstorff, P.; Fohlman, J. Proposal for a Common Nomenclature for Sequence Ions in Mass Spectra of Peptides. *Biomed. Mass Spectrom.* **1984**, *11* (11), 601. https://doi.org/10.1002/bms.1200111109.

(48) Biemann, K. Contributions of Mass Spectrometry to Peptide and Protein Structure. *Biomed. Environ. Mass Spectrom.* **1988**, *16* (1–12), 99–111. https://doi.org/10.1002/bms.1200160119.

(49) Chung, T. W.; Hui, R.; Ledvina, A.; Coon, J. J.; Turecek, F. Cascade Dissociations of Peptide Cation-Radicals. Part 1. Scope and Effects of Amino Acid Residues in Penta-, Nona-, and Decapeptides. *J. Am. Soc. Mass Spectrom.* **2012**, *23* (8), 1336–1350. https://doi.org/10.1007/s13361-012-0408-9.

(50) Ledvina, A. R.; Coon, J. J.; Tureček, F. Competitive Hydrogen Atom Migrations Accompaying Cascade Dissociations of Peptide Cation-Radicals of the $z^{+\bullet}$ Type. *Int. J. Mass Spectrom.* **2015**, No. 377, 44–53. https://doi.org/10.1016/j.ijms.2014.02.015.

(51) Oh, H. B.; Moon, B. Radical-Driven Peptide Backbone Dissociation Tandem Mass

Spectrometry. *Mass Spectrom. Rev.* **2015**, *34*, 116–132. https://doi.org/10.1002/mas.21426

(52) Paizs, B.; Suhai, S. Fragmentation Pathways of Protonated Peptides. *Mass Spectrom. Rev.* **2005**, *24* (4), 508–548. https://doi.org/10.1002/mas.20024.

(53) Canon, F.; Milosavljević, A. R.; Nahon, L.; Giuliani, A. Action Spectroscopy of a Protonated Peptide in the Ultraviolet Range. *Phys. Chem. Chem. Phys.* **2015**, *17* (17), 25725–25733. https://doi.org/10.1039/c4cp04762a.

(54) Laskin, J.; Yang, Z.; Ng, C. M. D.; Chu, I. K. Fragmentation of Alpha-Radical Cations of Arginine-Containing Peptides. *J. Am. Soc. Mass Spectrom.* **2010**, *21* (4), 511–521. https://doi.org/10.1016/j.jasms.2009.12.021.

(55) Wee, S.; O'Hair, R. A. J.; McFadyen, W. D. Comparing the Gas-Phase Fragmentation Reactions of Protonated and Radical Cations of the Tripeptides GXR. *Int. J. Mass Spectrom.* **2004**, *234* (1–3), 101–122. https://doi.org/10.1016/j.ijms.2004.02.018.

(56) Sun, Q.; Nelson, H.; Ly, T.; Stoltz, B. M.; Julian, R. R. Side Chain Chemistry Mediates Backbone Fragmentation in Hydrogen Deficient Peptide Radicals. *J. Proteome Res.* **2009**, *8* (2), 958–966. https://doi.org/10.1021/pr800592t.

(57) Neese, F. Software Update: The ORCA Program System, Version 4.0. *Wiley Interdiscip. Rev. Comput. Mol. Sci.* **2018**, *8* (1), 4–9. https://doi.org/10.1002/wcms.1327.

(58) A. D. Becke. Density-Functional Exchange-Energy Approximation with Correct Asymptotic Behavior. *Phys. Rev. A* **1988**, *4* (4), 276–282. https://doi.org/10.1063/1.1749835.

(59) Becke, A. D. Density-Functional Thermochemistry. III. The Role of Exact Exchange. *J. Chem. Phys.* **1993**, *98* (7), 5648–5652. https://doi.org/10.1063/1.464913.

(60) Weigend, F.; Ahlrichs, R. Balanced Basis Sets of Split Valence, Triple Zeta Valence and Quadruple Zeta Valence Quality for H to Rn: Design and Assessment of Accuracy. *Phys. Chem. Chem. Phys.* **2005**, *7* (18), 3297–3305. https://doi.org/10.1039/b508541a.

(61) Roemelt, M.; Maganas, D.; Debeer, S.; Neese, F. A Combined DFT and Restricted Open-Shell Configuration Interaction Method Including Spin-Orbit Coupling: Application to Transition Metal L-Edge X-Ray Absorption Spectroscopy. *J. Chem. Phys.* **2013**, *138* (20). https://doi.org/10.1063/1.4804607.

(62) Baerends, E. J.; Ellis, D. E.; Ros, P. Self-Consistent Molecular Hartree-Fock-Slater Calculations I. The Computational Procedure. *Chem. Phys.* **1973**, *2* (1), 41–51. https://doi.org/10.1016/0301-0104(73)80059-X.

(63) Dunlap, B. I.; Connolly, J. W. D.; Sabin, J. R. On Some Approximations in Applications of Xα Theory. *J. Chem. Phys.* **1979**, *71* (8), 3396–3402. https://doi.org/10.1063/1.438728.

(64) Vahtras, O.; Almlöf, J.; Feyereisen, M. W. Integral Approximations for LCAO-SCF Calculations. *Chem. Phys. Lett.* **1993**, *213* (5–6), 514–518. https://doi.org/10.1016/0009-2614(93)89151-7.

(65) Eichkorn, K.; Treutler, O.; Öhm, H.; Häser, M.; Ahlrichs, R. Auxiliary Basis Sets to Approximate Coulomb Potentials. *Chem. Phys. Lett.* **1995**, *240* (4), 283–290. https://doi.org/10.1016/0009-2614(95)00621-A.

(66) Eichkorn, K.; Weigend, F.; Treutler, O.; Ahlrichs, R. Auxiliary Basis Sets for Main Row Atoms and Transition Metals and Their Use to Approximate Coulomb Potentials. *Theor. Chem. Acc.* **1997**, *97* (1–4), 119–124. https://doi.org/10.1007/s002140050244.

(67) Stoychev, G. L.; Auer, A. A.; Neese, F. Automatic Generation of Auxiliary Basis Sets. *J. Chem. Theory Comput.* **2017**, *13* (2), 554–562. https://doi.org/10.1021/acs.jctc.6b01041.

(68) Van Lenthe, E.; Snijders, J. G.; Baerends, E. J. The Zero-Order Regular Approximation for Relativistic Effects: The Effect of Spin-Orbit Coupling in Closed Shell Molecules. *J. Chem. Phys.* **1996**, *105* (15), 6505–6516. https://doi.org/10.1063/1.472460.